Acta Geochim (2019) 38(6):848–862
https://doi.org/10.1007/s11631-019-00352-y

ORIGINAL ARTICLE

REE geochemistry of gangue minerals and their geological significance in the Muli antimony ore deposit in Yunnan, China

Zhenchun Han[1] · Jiasheng Wang[1] · Chao Li[2] · Kaidi Qiao[1] · Jinyang Chang[1]

Received: 17 September 2018 / Revised: 13 March 2019 / Accepted: 8 May 2019 / Published online: 17 May 2019

Abstract The Muli antimony deposit is located in the Au–Sb polymetallic metallogenic belt in south-eastern Yunnan, China. In this paper, we investigated the concentrations of trace elements in gangue minerals, mainly calcite, quartz, and pyrite, which were formed at different metallogenic stages. Meanwhile, the host rocks, predominantly composed of limestone, are also analysed for comparison. The calcite from the Nadan ore section is enriched with medium-heavy rare earth elements (M-HREEs), likely due to the presence of a high concentration of Fe and Mn impurities, which results in the preferential enrichment of M-HREEs in the calcite. Alternatively, the calcite may be precipitated from the M-HREE-rich granitic leaching fluid. In the Muli ore section, both quartz and pyrite in the metallogenic period show enrichment with light rare earth elements (LREEs), and the wall rock is also enriched with LREEs, which indicates that the wall rock material was involved in the metallogenic process. The W-shaped tetrad effect of quartz in the late metallogenic stage was interpreted to determine extensive fluid–rock interactions in highly fractionated Si-rich systems. Fe and Mn impurities cause M-HREE to be preferentially enriched with calcite to some extent. Whether mineralization is related to granite deserves further study. Eu and Ce anomalies of different types of gangue minerals indicate that the temperature and the fO_2 were constantly changing during mineralization, and the temperature of the main ore-stage was higher than 200 °C in an oxidized state. The various REE patterns, LREE/HREE and $(La/Yb)_N$ values, reveal that there may be multi-sources and multi-stage hydrothermal activities in the Muli antimony deposit. The REE distribution patterns of minerals are likely interfered with by many internal and external factors. Studies on REE characteristics of calcite, quartz, pyrite and limestone in the Muli antimony deposit have greatly improved the understanding of ore-forming fluids. When we traced the origin and evolution of ore-forming fluids by means of mineral REE distribution patterns, in addition to the determination of inclusions of ore minerals related to mineralization and the in situ analysis methods performed by LA-ICP-MS, we should also combine the REE characteristics of various minerals or trace the ore-forming fluids with multiple methods.

Keywords Muli antimony deposit · Ore-forming fluids · REE · Calcite · Pyrite · Quartz

1 Introduction

Geochemistry of rare earth elements (REEs) in hydrothermal minerals such as calcite (Yan et al. 2000; Feng et al. 2011; Wang et al. 2012b; Bao et al. 2013; Abedini et al. 2016), fluorite (Cao 1995; Cao et al. 2014; Shen et al. 2015; Li et al. 2015), quartz (Jiang 1988; Fan et al. 2000; Zhang et al. 2011; Wang et al. 2015) and pyrite (Li et al. 2003; Chen et al. 2007; Zhang et al. 2012), plays a crucial role in tracing the origin and evolution of ore-forming fluids (Lottermoser 1992; Whitney and Olmsted 1998; Hecht et al. 1999; Ghaderi et al. 1999; Wang et al.

✉ Jiasheng Wang
jiashengwang@126.com

✉ Chao Li
Re-Os@163.com

[1] Southwest Institute of Geological Survey, Kunming University of Science and Technology, Kunming 650093, China

[2] National Research Center for Geoanalysis, Beijing 100037, China

2003; Peng et al. 2006; Liang et al. 2007). REEs can be enriched in these minerals by several processes, including sorption, complexation, coprecipitation, and fluid inclusion (Debruyne et al. 2016). Medium-heavy rare earth elements (M-HREEs) including can be enriched in calcium minerals such as calcite (Wang et al. 2012b), fluorite (Chesley et al. 1991, 1994; Peng et al. 2003) and scheelite (Roberts et al. 2006; Leng et al. 2018), which can provide insights into mineralization ages due to their high Sm and Nd contents and high Sm/Nd ratios. YREE (REE + yttrium) patterns in calcite can be used to assess stadial-interstadial changes (Zhou et al. 2012). Fan et al. (2000) reported that the REE pattern of quartz is similar to that of fluid inclusions, suggesting that the REEs in quartz are concentrated in fluid inclusions and represent the characteristics of quartz-forming fluids. The study on the REE characteristics of gangue calcites and host rocks published by Deng et al. (2014) indicates that the ore-forming fluids are of the crustal type. Hence, the chemical properties of REE and combined yttrium (YREE), which act as geochemical tracers, have been widely studied to better understand metallogenic mechanisms.

Various types of hydrothermal deposits, such as Hg, Zn-Pb, Sb and Au deposits, have been extensively developed in the large-scale low-temperature epithermal metallogenic domain in southwestern China (Fig. 1). The geochemical characteristics of REE in calcite, fluorite, quartz and other gangue minerals in various types of deposits in this metallogenic domain have been previously studied. The results show that the REE patterns of metallogenic calcite or fluorite in mercury deposits (Wang et al. 2010; Han et al. 2017) and Pb–Zn deposits (Huang et al. 2001; Bao et al. 2013) are characterized by an enrichment with light rare earth elements (LREE), such as the La'e Mercury deposit, Huize deposit and the Maozu Pb–Zn deposit; the metallogenic calcites in antimony deposits are enriched with M-HREEs, such as the Xikuangshan deposit (Peng et al. 2004), the Banpo deposit (Deng et al. 2014), and the Qinglong deposit (Wang et al. 2003, 2011; Zhu et al. 2010); the metallogenic calcites of Carlin-type gold deposits are mainly enriched with MREEs, such as the Bojitian deposit (Zhang et al. 2010), the Taipingdong-Zimudang deposits (Wang et al. 2012b), the Shuiyindong deposit (Su et al. 2009) and the Getang deposit (Huang et al. 2012). Additionally, the same minerals formed at different metallogenic stages have different REE patterns, and different minerals in the same deposit also present different REE patterns (Hazarika et al. 2016; Peng et al. 2004; Wang et al. 2012b; Zhang et al. 2010).

Although the REE chondrite-normalized patterns of gangue minerals from hydrothermal ore deposit have been widely studied to determine the origin of hydrothermal fluids or as a sensitive indicator of hydrothermal systems, some issues still need to be addressed. When multiple REE patterns occur in different minerals or even in the same minerals at different metallogenic stages, which mineral can be used for direct tracing? Or under which conditions can these hydrothermal minerals be used in tracing?

In the present study, REE patterns of calcite, quartz, pyrite and wall rocks from the Muli antimony deposit were studied. This study aims to discuss the feasibility of using the REE patterns of gangue minerals to trace the ore-forming fluids and illustrate the origin and evolution of ore-forming fluids in the Muli antimony deposit.

2 Geological setting

The Muli antimony ore deposit belongs to the polymetallic metallogenic belt of the south-eastern Yunnan province, and it is tectonically located in the Qiubei-Guangnan fold bundles of the south-eastern Yunnan fold belt in the South China fold system (Wang and Man 1994). The deposit is trapped in the complex fold belt between the Xiaopunong thrust fault and the Nawai thrust fault (Fig. 2). The geological structure in the ore district is arc distributed with a north-west direction, and it is dominated by fold structures. There are a series of NE-trend faults in the west, first turning to near EW-trend direction, and then following the NW-trend direction. The main anticlines in this area are the Muli-Nadan anticline, the Ankang anticline, the Dianzhan anticline, the Nonglang anticline, and so on. The brittle rocks such as silexite are broken during the fold formation, which provides a good space for mineralization. In addition, a series of compression-torsional faults have been developed, such as the Nawai fault and the Xiaopunong fault (Fig. 3), which provide a suitable place for migration and enrichment of ore-forming fluids. The stratigraphy of the mining area is semi-deep to shallow water shelf facies (Huang and Lei 1997). The strata cropping out in this area range from Lower Devonian to Middle Triassic, but the Lower Triassic is absent (Fig. 4). The Pojiao (D_1p) formation acts as the main ore-hosting strata and is composed of thick-bedded silexite, with thin-bedded planktonic and benthic sedimentary biogenic limestone and local chert nodules and limestone lens. The Bajiaoqing (D_1b), Pozheluo (D_2p), Donggangling (D_2d), Wuzhishan and Liujiang ($D_3l + w$) formations are mainly composed of thin-bedded silexite, shale and dolomitic limestone. The Baifeng ($T_{2-}b$) formation consists of fine-sandstone and sandy shale, and usually occurs as the hanging wall of the ore body (Li 1999; Yu 1990).

There are different ore types in the Nadan and Muli ore sections. The Nadan ore section is mainly composed of stibnite and calcite symbiotic association. Quartz and pyrite are less developed, and calcite formation is closely

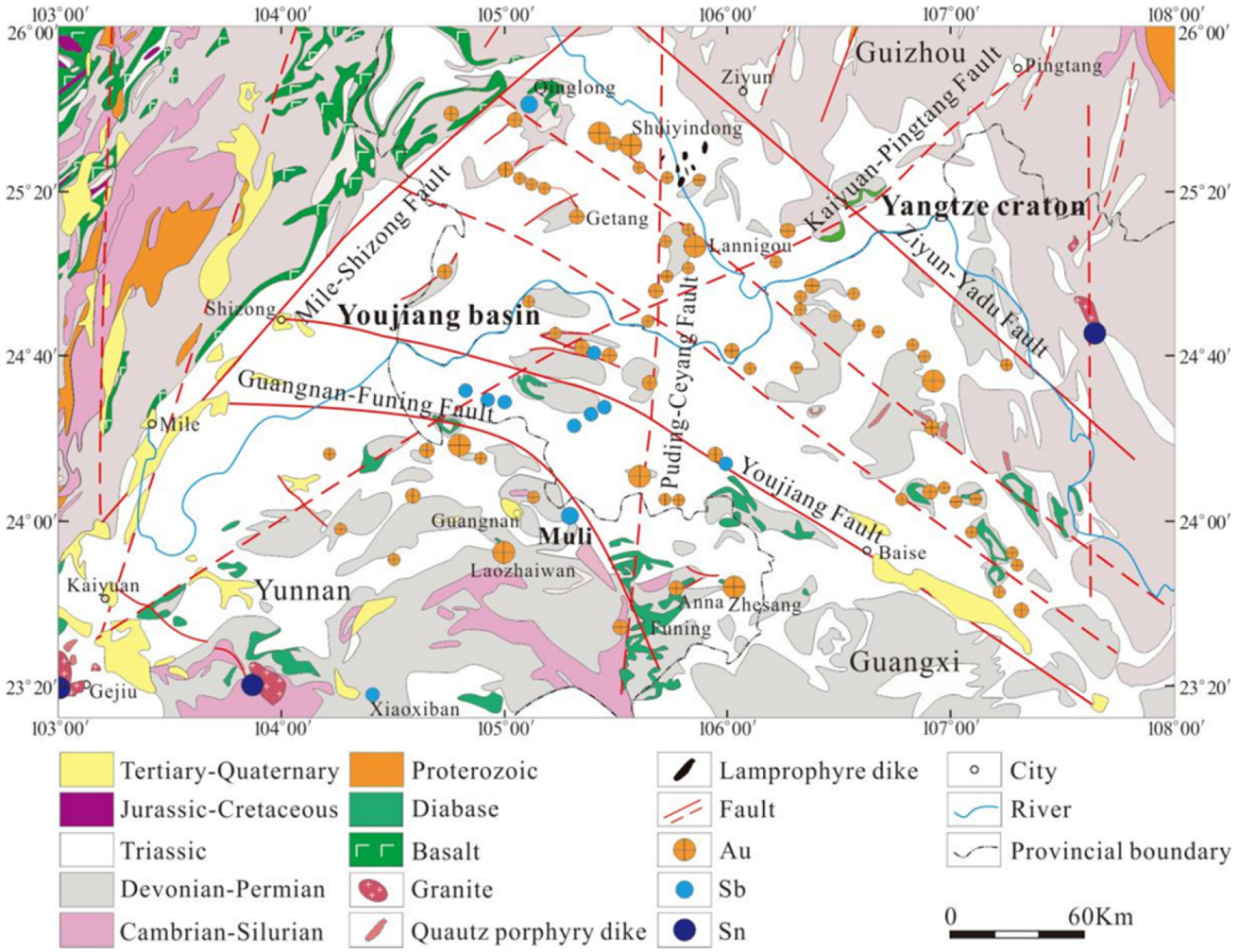

Fig. 1 Geologic map of the large-scale low-temperature epithermal metallogenic domain in southwestern China, showing the locations of Carlin-type gold, antimony and tin-polymetallic deposits in the Youjiang basin (modified after Su et al. 2018)

related to mineralization (Fig. 5a, b). The Muli ore section is characterized by a mineral symbiotic association of stibnite, pyrite and quartz (Fig. 5c–e). A green quartz vein develops in late metallogenic structure, with minor pyritization (Fig. 5f). Calcite of late metallogenic stage occurs in a metallogenic fault structure, and extensive Sb mineralization is developed in the upper wall of fault; however, calcite is formed later than the symbiotic association of stibnite, quartz and pyrite (Fig. 5g). The post-metallogenic calcite emerges in post-metallogenic fault structure, and there is no mineralization near the fault after mineralization (Fig. 5h).

Based on mineral paragenesis, we present a mineral paragenetic sequence of the Muli antimony deposit in Fig. 6. Hydrothermal alteration is typically composed of calcification, silicification and weak bituminization. Calcite and quartz are the predominant gangue minerals.

3 Sampling and analytical methods

Calcite, quartz, pyrite and limestone from the Nadan and Muli ore sections of the Muli antimony deposit were sampled with detailed information of sample locations and characteristics shown in Table 1. Field characteristics and microscopic features of hand specimens are shown in Fig. 5.

Different minerals were handpicked under a binocular microscope, and impurities were removed. The purity of the collected samples was over 99%. The REE concentrations of the studied samples were carried out at the National Research Centre for Geoanalysis. For calcite and pyrite, the specific operating procedures are as follows: 25 mg pulverized samples of calcites and pyrites (200 mesh) were placed in 10 mL Teflon hexagonal bottles and digested with 0.5 mL of 10 mol/L HCl and 1.5 mL of 15 mol/L HNO_3 overnight, and then the samples were heated at 130 °C for 16 h. After sample solutions were

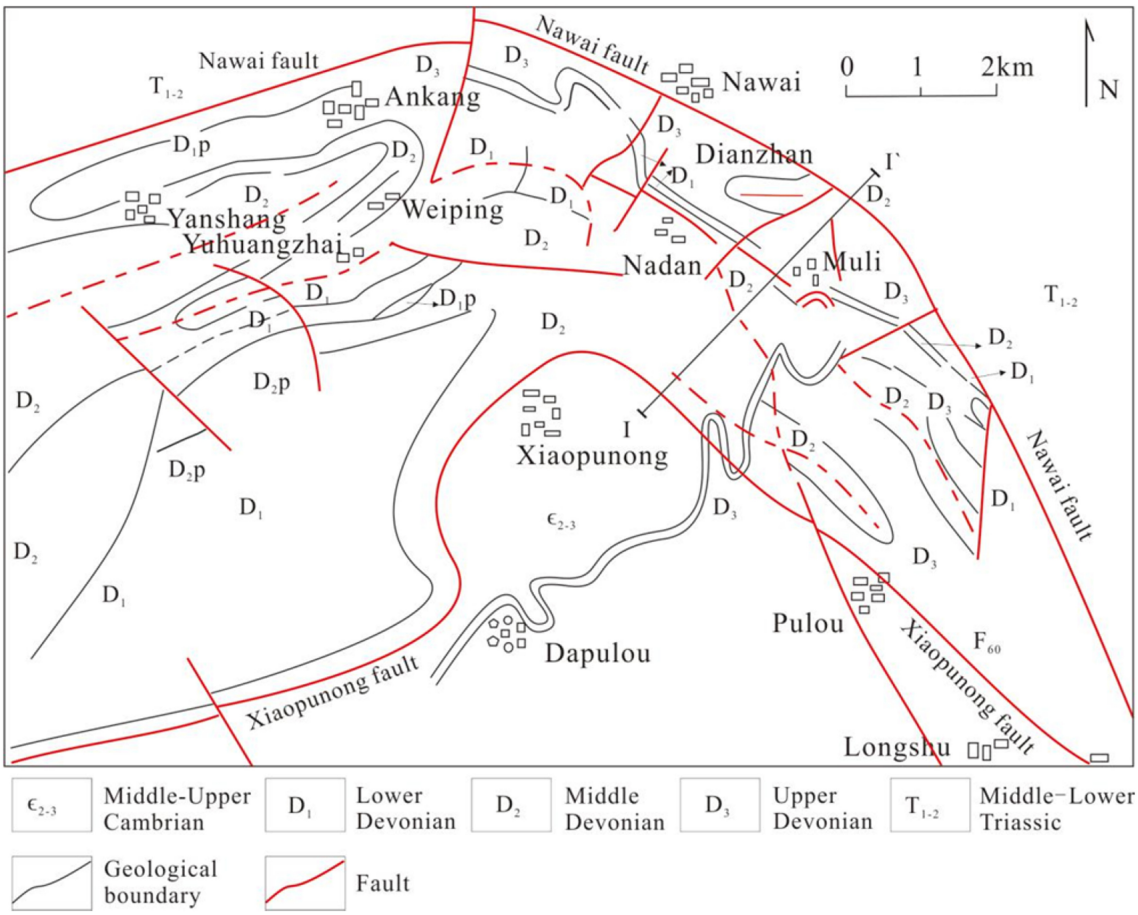

Fig. 2 Geological map of the Muli antimony ore deposit in Yunnan

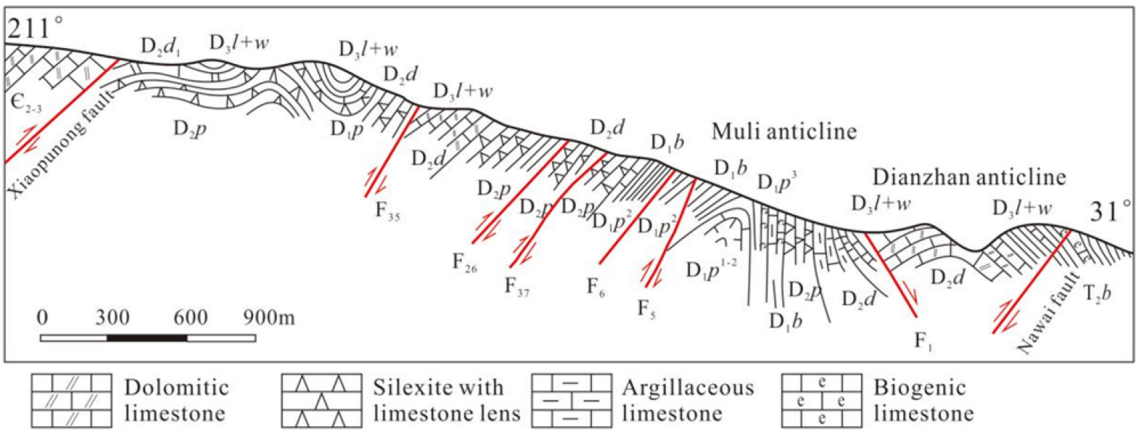

Fig. 3 Geological section map (I–I′) of the Muli antimony ore deposit in Yunnan

evaporated to near dryness at 150 °C on a hot plate, the dissolved solutions were transferred to colorimetric tubes and diluted to 25 mL using ultrapure water. For 50 mg quartz and limestone samples, 1 mL HF and 0.5 mL HNO_3 was added into the Teflon bomb and heated at 190 °C for 24 h. After the sample solution was evaporated to dryness at 200 °C on a hot plate, 0.5 mL of HNO_3 was added. After adding 2.5 mL of HNO_3, the Teflon bomb was sealed and heated at 130 °C for 5 h. After cooling, the solutions were transferred to a plastic bottle and diluted with ultrapure water to 50 mL. The sample solutions were determined by an inductively-coupled plasma mass spectrometer (ICP-MS, NexION 350, PerkinElmer, USA). Analytical accuracy for trace elements is higher than five relative percent.

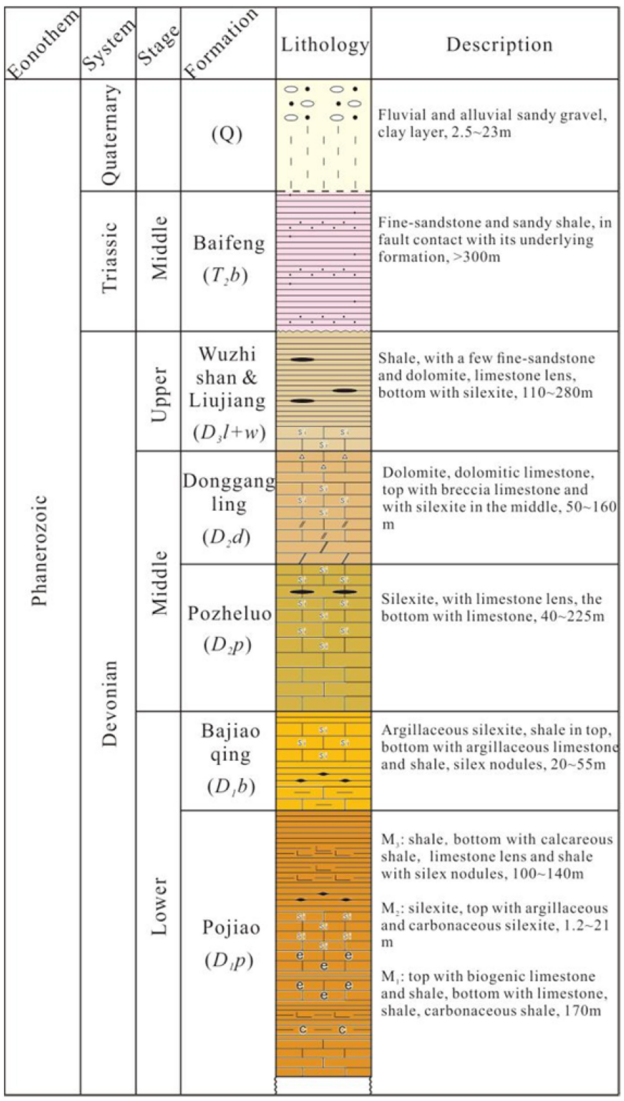

Fig. 4 The stratigraphic column of the Muli antimony deposit in Yunnan

4 Analytical results

A total of 15 calcite samples, 2 pyrite samples, 5 quartz samples and 2 limestone samples from the Muli antimony deposit were measured. The contents and characteristic parameters of rare earth elements in each sample are shown in Table 2.

The REE patterns of quartzes formed during the metallogenic period and late metallogenic stage from the Muli ore section are shown in Figs. 7 and 8. The metallogenic stage quartzes are characterized by enrichment in LREE. The total REE (excluding Y, as below) contents range from 0.19 to 1.24 μg/g, the ratio of LREE/HREE is in the range of 11.70–76.69, and there are weak positive Eu and negative Ce anomalies (δCe = 0.76–0.83). The late metallogenic stage quartzes are enriched in MREE with ∑REE = 0.24–3.16 μg/g, LREE/HREE = 0.71–1.84, and both with negative Eu and Ce anomalies (δEu = 0.62–0.86, δCe = 0.28–0.71). The REE pattern of calcite (ML-21) precipitated in the late metallogenic stage is characterized by M-HREE enrichment with ∑REE = 3.82 μg/g and negative Eu and Ce anomalies (Fig. 8).

Calcites formed at the post-metallogenic period in the Muli ore section have the characteristics of the right-inclined type with LREE enrichment (Fig. 9). The total REE concentrations of ML-16 and ML-19 are slightly low, while ML-15 has higher REE concentrations. ML-16 exhibits a weak negative Eu anomaly, while ML-19 displays an extremely positive Eu anomaly.

The REE patterns of pyrite are very similar to those of limestone in the Muli ore section (Figs. 10, 11) and exhibit LREE enrichment. The fractionation of LREE and HREE in pyrite is apparent, with ∑REE = 3.50–8.46 μg/g, LREE/HREE = 5.57–11.88; however, the Eu and Ce anomalies are not evident. The fractions of LREE and HREE in limestones are also distinct with ∑REE = 13.15–72.19 μg/g, and LREE/HREE = 3.24–9.14. The samples also show a negative Eu anomaly but a minor Ce anomaly.

The REE patterns of metallogenic calcite of the Nadan ore section are shown in Fig. 12. The REE contents of ND-13 and ND-22, 11.07 μg/g and 14.80 μg/g, respectively, are slightly higher than other sample values. ∑REE values of other calcite samples range from 2.05 to 5.29 μg/g. The calcites display M-HREE enrichment with LREE/HREE = 0.38–1.01 and weak negative Eu and Ce anomalies (δEu = 0.72–0.89, δCe = 0.45–0.91).

5 Discussion

5.1 Enrichment mechanism of REE in quartz, pyrite and calcite

The radius of Si^{4+} (0.41 Å) is much smaller than those of REE^{3+}, which means that REEs cannot enter the quartz lattice in the form of isomorphic substitution but only as fluid inclusions in quartz (Norman and Landis 1983; Fan et al. 2000). Therefore, quartz should directly record the REE geochemical characteristics of ore-forming fluids at the time of crystallization. Fe and REE have completely different geochemical affinities. In addition, the radii of Fe^{2+} (0.76 Å) and REE^{3+} (0.98–1.16 Å) are quite different from each other, so it is impossible for REEs to get into pyrite as a homologue. It is believed that REEs occur in the form of inclusions in pyrite or in its lattice defects (Bi et al. 2004; Chen et al. 2007). Therefore, the geochemical signatures of REEs in pyrite during the hydrothermal metallogenic period can be an indicator to be used to track fluid

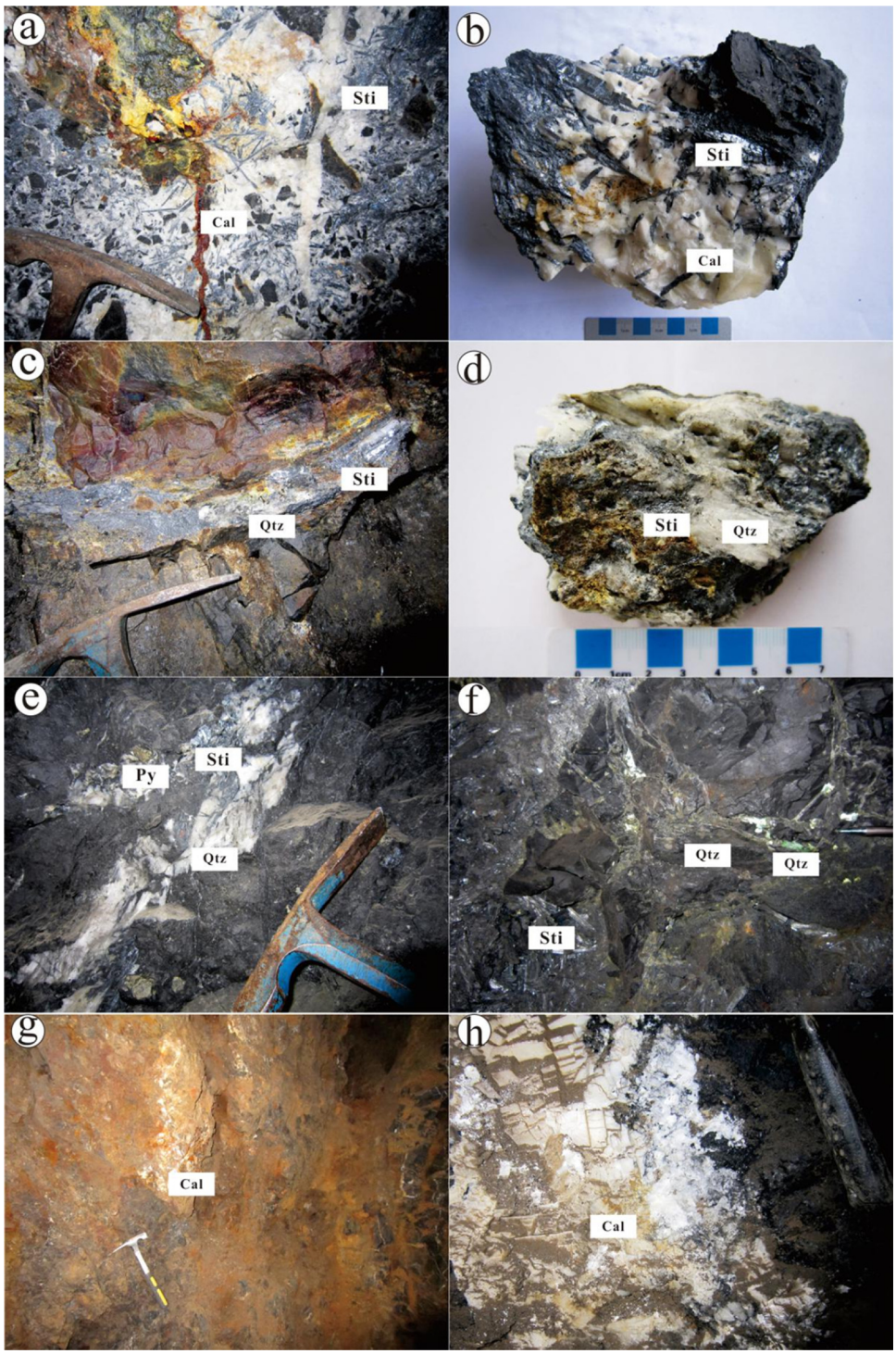

Fig. 5 **a**, **b.** A symbiotic association of stibnite and calcite in the metallogenic stage; **c**, **d.** a symbiotic association of stibnite and quartz in the metallogenic stage; **e.** pyrite in the metallogenic stage; **f.** green quartz in the late metallogenic stage; **g.** calceite in the late metallogenic stage; **h.** Calcite in the post-metallogenic stage. **a**, **b** are from the Nadan ore section; **c**–**h** are from the Muli ore section

conditions at the time of crystallization. Mao et al. (2006) proposed that the silicate phase in pyrite can influence the contents and features of REE in pyrite, suggesting that eliminating the influence of the silicate phase in pyrite is an essential precondition for tracing. In the present experiment, aqua regia was used to dissolve pyrite, silicate phase in the pyrite was not digested, and therefore, features in pyrite should not be disturbed by the REE characteristics of the silicate phase.

Quartz formed at the late metallogenic stage displays the tetrad effects of a W-shaped chondrite-normalized pattern. This type of REE pattern typically occurs in highly evolved silicate magma (i.e., granites) (Schönenberger et al. 2008; Takahashi et al. 2002). Veksler et al. (2005) proposed that

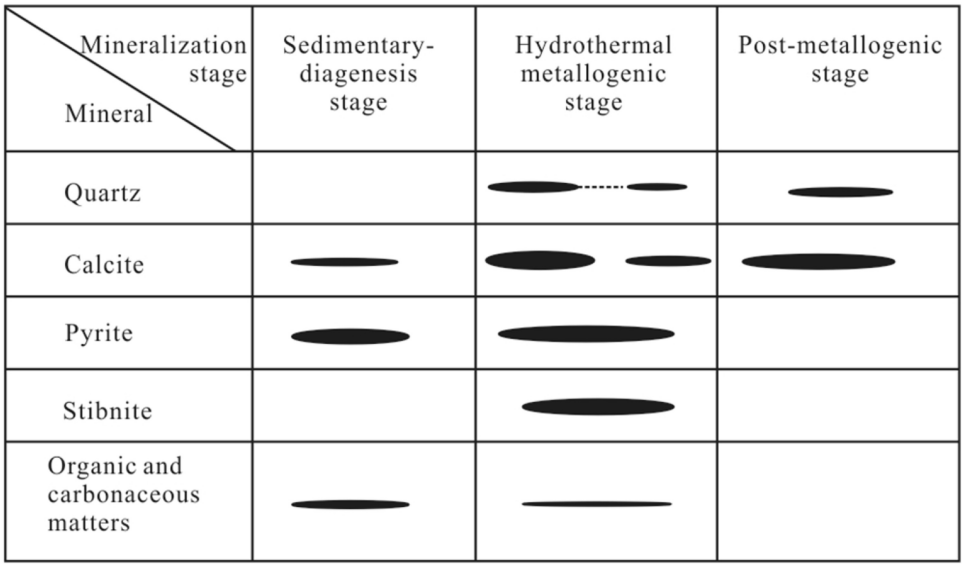

Fig. 6 The mineral paragenetic sequence of major minerals from the Muli antimony deposit in Yunnan

Table 1 Sample information of calcites from the Muli antimony deposit in Yunnan

Mineral/rock	Sample no.	Occurrence	Colour	Metallogenic stage
Calcite	ND-1	Vein, massive	White, pink	Metallogenic
	ND-3		White, pink, buff	
	ND-4			
	ND-5			
	ND-8	Vein	White	
	ND-11		Pink	
	ND-13	Vein, massive	White, pink, buff	
	ND-16		White, milky, pink	
	ND-19c		White, milky	
	ND-22		White, milky, pink	
	ND-23		White, milky	
Quartz	ML-11	Vein	Green	Late metallogenic
	ML-12			
	ML_2-2	Vein	White	Metallogenic
	ML_2-7b			
	ZK201-14			
Pyrite	ML-8	Massive	–	Metallogenic
	ML-66	Massive	–	
Calcite	ML-15	Vein	White, milky	Post-metallogenic
	ML-16			
	ML-19			
	ML-21	Vein, massive	White, isabelline	Late metallogenic
Limestone	ML-7	–	Grey black	–
	ML-17	–		–

silicate melts produce M-shaped tetrad effects. However, when combined with fluoride-bearing fluids, silicate melts should have a W-shape. Zhao et al. (1992, 2002) found that the dominant minerals and REE-bearing accessory minerals in the granite-related rare metal deposits in South China have M-shaped tetrad effects.

The genesis of the REE fractionation in calcite is complex. REEs mainly enter calcite ($CaCO_3$), fluorite (CaF_2), scheelite ($CaWO_4$), apatite ($Ca_5[PO_4]_3$) and other calcium-bearing minerals by replacing Ca^{2+} in the lattice. It is easier for LREEs such as La^{3+} (ionic radius of 6-fold coordination is 1.03 Å) to replace Ca^{2+} with an ionic

Table 2 REE contents (ppm) and statistical parameters of calcites, quartzes, pyrites and limestones from the Muli antimony deposit in Yunnan

Mineral/rock	Ore stage	Sample no.	La	Ce	Pr	Nd	Sm	Eu	Gd	Tb	Dy	Ho	Er	Tm	Yb
Calcite	Metallogenic	ND-1	0.07	0.17	0.04	0.36	0.23	0.08	0.44	0.07	0.57	0.13	0.37	0.05	0.26
		ND-3	0.13	0.35	0.09	0.67	0.33	0.11	0.55	0.09	0.66	0.15	0.43	0.05	0.29
		ND-4	0.10	0.28	0.07	0.46	0.21	0.08	0.32	0.05	0.34	0.08	0.20	0.03	0.13
		ND-5	0.06	0.14	0.04	0.31	0.20	0.07	0.40	0.07	0.54	0.12	0.36	0.04	0.23
		ND-8	0.12	0.27	0.06	0.44	0.37	0.18	1.01	0.18	1.20	0.26	0.68	0.09	0.53
		ND-11	0.07	0.20	0.05	0.43	0.26	0.09	0.50	0.08	0.61	0.14	0.40	0.05	0.28
		ND-13	0.51	1.32	0.28	1.72	0.90	0.34	1.63	0.27	1.79	0.37	1.04	0.14	0.84
		ND-16	0.07	0.17	0.04	0.35	0.25	0.10	0.47	0.08	0.53	0.12	0.33	0.04	0.26
		$ND\text{-}19_C$	0.12	0.16	0.04	0.31	0.23	0.10	0.48	0.09	0.63	0.14	0.41	0.06	0.34
		ND-22	0.57	1.56	0.34	2.12	1.14	0.43	2.23	0.37	2.52	0.52	1.49	0.20	1.29
		ND-23	0.07	0.15	0.03	0.21	0.14	0.06	0.33	0.06	0.46	0.10	0.30	0.04	0.24
	Late-metallogenic	ML-21	0.20	0.29	0.06	0.38	0.23	0.10	0.56	0.11	0.76	0.17	0.47	0.03	0.22
	Post-metallogenic	ML-15	3.41	6.21	0.73	2.65	0.53	0.20	0.71	0.10	0.56	0.10	0.28	0.01	0.09
		ML-16	0.56	1.03	0.14	0.59	0.16	0.05	0.25	0.03	0.22	0.04	0.11	0.01	0.04
		ML-19	0.94	1.80	0.24	0.98	0.18	0.65	0.22	0.03	0.14	0.02	0.06	0.06	0.37
Quartz	Metallogenic	$ML_2\text{-}7b$	0.05	0.07	0.01	0.04	0.01	–	–	–	–	–	–	–	0.01
		ZK201-14	0.40	0.53	0.03	0.14	0.12	–	0.01	–	0.01	–	–	0.03	0.20
	Late-metallogenic	ML-11	0.04	0.05	0.01	0.03	0.02	0.01	0.03	–	0.03	–	0.01	–	0.01
		ML-12	0.64	0.28	0.05	0.41	0.27	0.09	0.44	0.07	0.39	0.07	0.18	–	–
		$ML_2\text{-}2$	0.01	0.02	0.01	0.04	0.02	0.01	0.06	0.01	0.04	0.01	0.02	–	–
Pyrite	Metallogenic	ML-8	1.98	3.62	0.41	1.44	0.28	0.07	0.22	0.03	0.15	0.03	0.10	0.01	0.10
		ML-66	0.65	1.24	0.15	0.66	0.20	0.07	0.19	0.03	0.15	0.03	0.06	0.01	0.06
Limestone		ML-7	14.83	29.31	3.43	13.57	3.22	0.75	3.13	0.35	1.72	0.29	0.83	0.10	0.62
		ML-17	2.41	4.26	0.52	2.19	0.58	0.13	0.89	0.14	0.85	0.17	0.50	0.07	0.44

Mineral/rock	Ore stage	Sample no.	Lu	Y	ΣREE	LREE	HREE	LREE/HREE	La_N/Yb_N
Calcite	Metallogenic	ND-1	0.03	7.82	2.88	0.96	1.93	0.50	0.18
		ND-3	0.04	8.19	3.96	1.68	2.28	0.74	0.30
		ND-4	0.02	4.06	2.38	1.21	1.17	1.03	0.54
		ND-5	0.03	7.74	2.62	0.82	1.80	0.45	0.17
		ND-8	0.08	14.73	5.48	1.45	4.03	0.36	0.15
		ND-11	0.04	8.28	3.21	1.11	2.09	0.53	0.18
		ND-13	0.12	18.44	11.25	5.06	6.20	0.82	0.41
		ND-16	0.04	6.10	2.85	0.98	1.87	0.52	0.17
		$ND\text{-}19_C$	0.05	6.72	3.15	0.95	2.19	0.44	0.24
		ND-22	0.19	24.18	14.99	6.18	8.81	0.70	0.30
		ND-23	0.03	5.38	2.23	0.67	1.57	0.43	0.20
	Late-Metallogenic	ML-21	0.05	7.87	3.82	1.28	2.54	0.50	0.37
	Post-Metallogenic	ML-15	0.03	4.44	15.77	13.72	2.04	6.72	10.27
		ML-16	0.01	1.99	3.29	2.52	0.77	3.26	4.27
		ML-19	–	1.10	5.32	4.79	0.53	9.01	14.27
Quartz	Metallogenic	$ML_2\text{-}7b$	–	0.03	0.19	0.17	0.01	11.70	13.72
		ZK201-14	–	0.09	1.24	1.23	0.02	76.69	85.58
	Late-Metallogenic	ML-11	–	0.11	0.24	0.15	0.08	1.84	2.96
		ML-12	0.04	1.87	3.16	1.75	1.41	1.24	2.11
		$ML_2\text{-}2$	–	0.28	0.24	0.10	0.14	0.71	1.00

Table 2 continued

Mineral/rock	Ore stage	Sample no.	Lu	Y	ΣREE	LREE	HREE	LREE/HREE	La_N/Yb_N
Pyrite	Metallogenic	ML-8	0.01	0.91	8.46	7.81	0.66	11.88	13.87
		ML-66	0.01	0.70	3.50	2.97	0.53	5.57	7.01
Limestone		ML-7	0.09	7.56	72.24	65.11	7.13	9.14	16.21
		ML-17	0.06	6.39	13.20	10.09	3.11	3.24	3.74

Mineral/rock	Ore stage	Sample no.	δEu	δCe	La/Ho	Y/Ho	$(Yb/La)_N$	$(Yb/Ca)_N$ (10^{-8})
Calcite	Metallogenic	ND-1	0.80	0.71	0.33	65.00	5.22	15.03
		ND-3	0.82	0.70	0.71	58.36	2.33	16.76
		ND-4	0.92	0.73	1.14	57.71	1.31	7.51
		ND-5	0.78	0.66	0.27	70.18	6.16	13.29
		ND-8	0.86	0.76	0.36	58.84	4.73	30.63
		ND-11	0.75	0.73	0.31	63.54	5.62	16.18
		ND-13	0.84	0.81	1.30	49.78	1.41	48.55
		ND-16	0.83	0.73	0.36	55.18	5.22	15.03
		$ND\text{-}19_C$	0.87	0.54	0.69	51.54	3.04	19.65
		ND-22	0.82	0.80	1.06	47.37	1.92	74.57
		ND-23	0.88	0.80	0.44	59.56	4.82	13.87
	Late-Metallogenic	ML-21	0.83	0.62	1.12	46.24	1.56	21.39
	Post-Metallogenic	ML-15	1.01	0.89	33.90	44.30	0.05	12.72
		ML-16	0.73	0.86	13.75	49.50	0.13	5.20
		ML-19	9.91	0.88	46.50	54.50	0.03	2.31
Quartz	Metallogenic	ML_2-7b	1.55	0.76				
		ZK201-14	0.51	0.83				
	Late-Metallogenic	ML-11	0.86	0.71				
		ML-12	0.79	0.28				
		ML_2-2	0.62	0.67				
Pyrite	Metallogenic	ML-8	0.84	0.90				
		ML-66	1.06	0.91				
Limestone		ML-7	0.72	0.94				
		ML-17	0.56	0.86				

Note: "–" means below the limit of detection

radius of 1.12 Å than it is for HREEs such as Lu^{3+} (ionic radius of 6-fold coordination is 0.86 Å). Therefore, theoretically, the partition coefficient $K_D^{REE\text{-}Ca}$ of REE in calcium-bearing mineral-fluid system decreases with the increase of the atomic number of REE (Rimstidt et al. 1998). Johannesson et al. (1996) proposed that solid–liquid exchange reactions or dissolution of surface Fe–Mn coatings, suspended particulates, and/or secondary phases as well as sulphate complexation, are more likely to control the development of MREE enrichment in natural acidic terrestrial waters. Leybourne et al. (2000) concluded that REEs are removed from solution by absorption to Fe- and Mn-oxyhydroxides in the order MREE ≥ LREE ≥ HREE. Peng et al. (2004) proposed that the optimum ion radius of a substitutional site for the REEs in hydrothermal calcites is approximately 0.091 ± 0.001 nm, which is close to the ionic radius of MREE and HREE but smaller than the theoretical value of the ideal Ca^{2+} ion. Wang et al. (2012b) explained that M-HREEs are preferentially incorporated into early precipitated calcite, resulting in their depletion of the hydrothermal fluids during later precipitation of calcite. Wang et al. (2018) showed that the contents of Fe and Mn in calcite of different stages are completely inconsistent, and that the Fe and Mn impurities in calcite may be the dominant mechanism that controls the distribution of M-HREEs in calcite. Mucci (1988) and Pingitore et al.

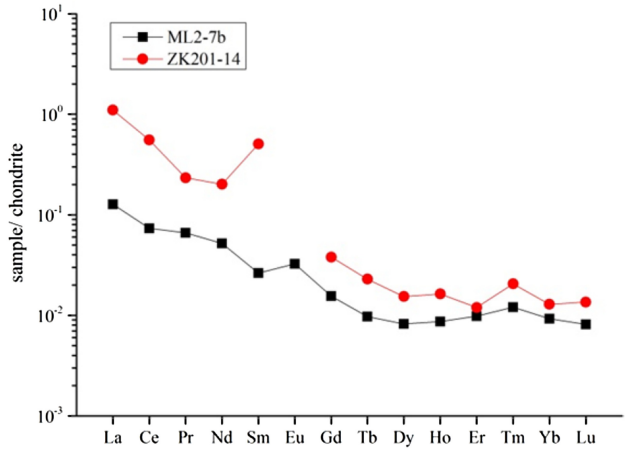

Fig. 7 Chondrite-normalized REE distribution patterns of quartzes in the metallogenic stage from the Muli ore section

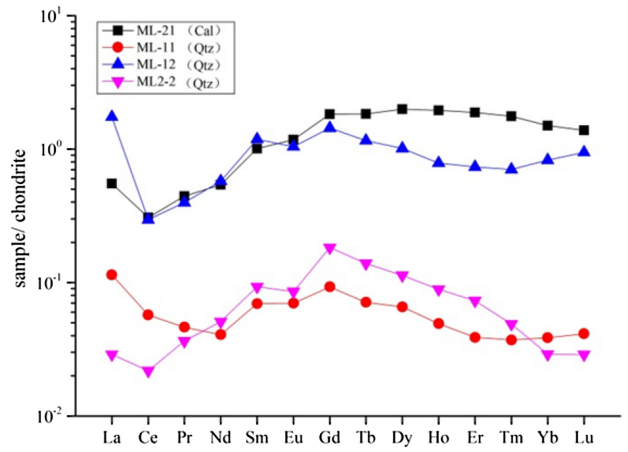

Fig. 8 Chondrite-normalized REE distribution patterns of quartzes and calcites in the late metallogenic stage from the Muli ore section

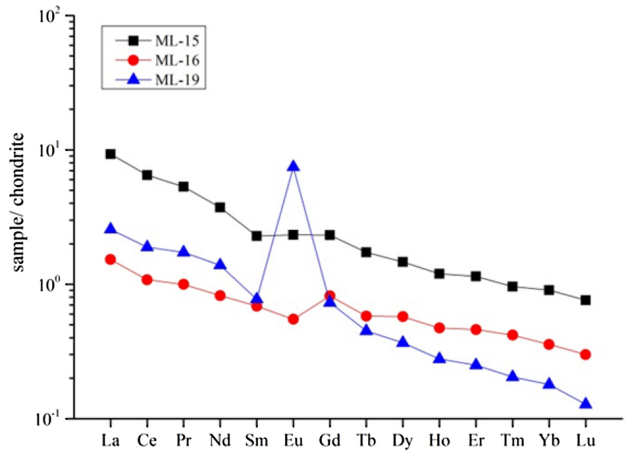

Fig. 9 Chondrite-normalized REE distribution patterns of calcites in the post-metallogenic stage from the Muli ore section

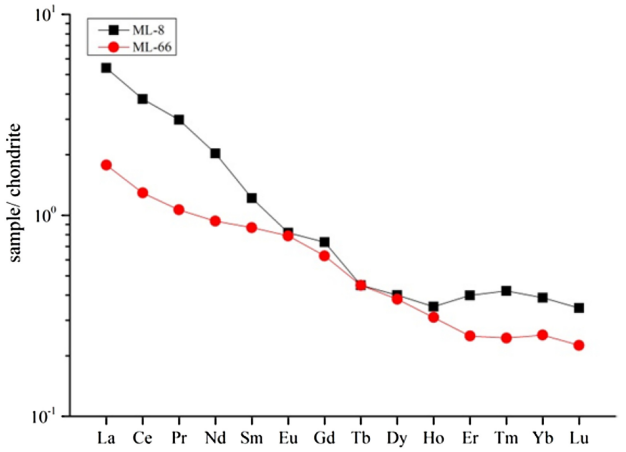

Fig. 10 Chondrite-normalized REE distribution patterns of pyrites in the metallogenic stage from the Muli ore section

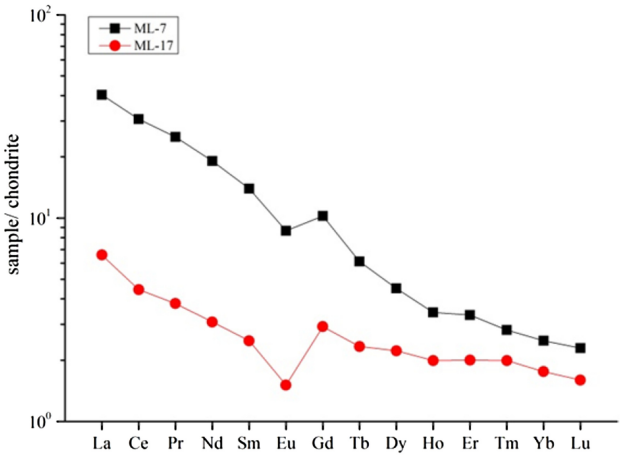

Fig. 11 Chondrite-normalized REE distribution patterns of limestones from the Muli ore section

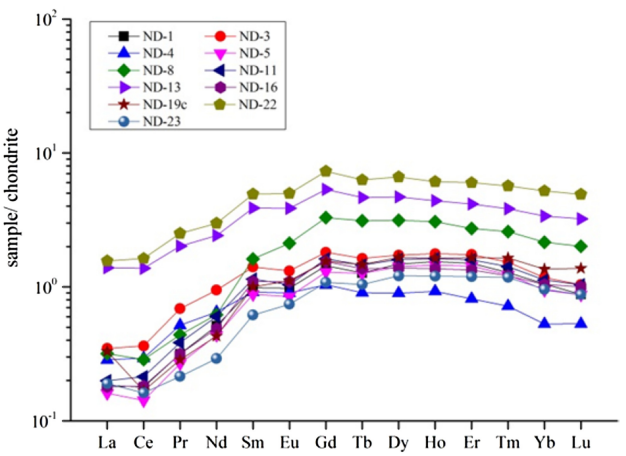

Fig. 12 Chondrite-normalized REE distribution patterns of calcites in the metallogenic stage from the Nadan ore section

(1988) have proved that the partition coefficients of Mn^{2+} under 25 °C decrease with the increase of calcite precipitation rate. Dromgoole and Walter (1990) hold that the interpretation of diagenesis can be effectively guided only if all the factors that control Mn^{2+} and Fe^{2+} incorporation are adequately constrained. Previous studies have also shown that Fe–Mn substances in calcite may play an important role in the enrichment of M-HREEs in calcites (Johannesson et al. 1996; Leybourne et al. 2000; Wang et al. 2012b).

5.2 Yb/Ca versus Yb/La and Y/Ho versus La/Ho

Since Yb/Ca and Yb/La ratios can be used to trace the formation environment and fractionation degree of calcite (Moller and Morteani 1983; Subías and Fernández-Nieto 1995), such ratios have been widely used in different types of ore deposits to investigate the ore genesis of these deposits. In this study, the values of these ratios have been plotted in Fig. 13. The results show that all calcite samples fall into the hydrothermal field, indicating that calcites have a hydrothermal origin. Bau and Dulski (1995) proposed that the homologous gangue minerals are distributed horizontally in the Y/Ho-La/Ho diagram. The Y/Ho and La/Ho ratios of calcites from the Muli antimony deposit also show similar features (Fig. 14), but the metallogenic calcites are separated from calcites in the post-metallogenic stage. Y/Ho versus La/Ho ratios imply that the metallogenic calcites from the Nadan ore section are homologous with those from the Muli ore section. Nevertheless, the varying La/Ho ratios of calcites in metallogenic and post-metallogenic stages indicate that the Muli ore section involves multi-stage hydrothermal activity.

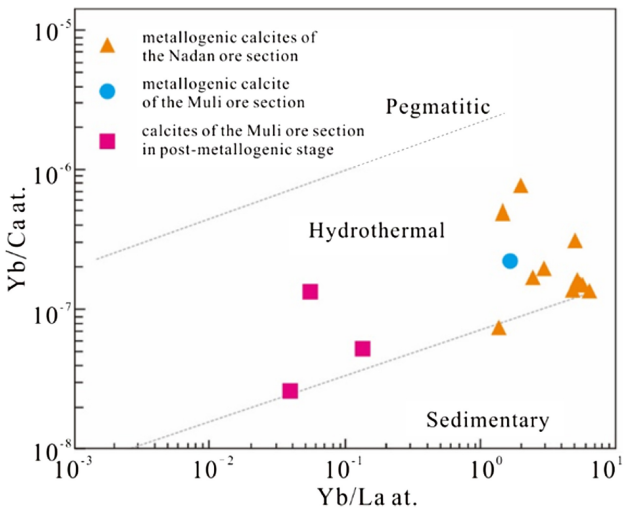

Fig. 13 Logarithmic plots of Yb/Ca versus Yb/La in calcites from the Muli antimony deposit

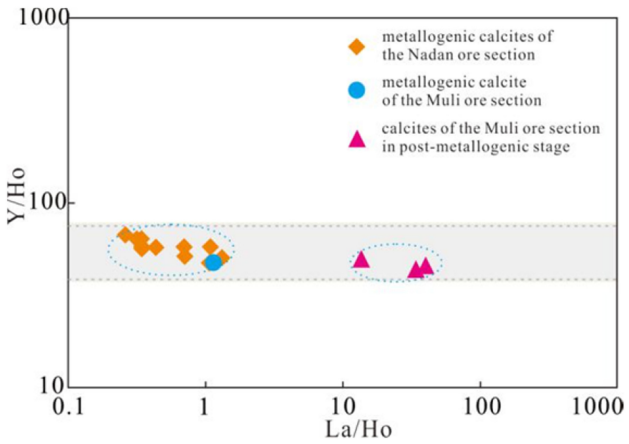

Fig. 14 Y/Ho versus La/Ho in calcites from the Muli antimony deposit

5.3 Eu and Ce anomalies

Eu anomalies in calcite can be achieved by the replacement of Ca^{2+} in calcite, fluorite and other calcium minerals. In the relatively oxidative environment, Eu replaces the Ca^{2+} in the form of Eu^{3+} and leads to a positive Eu anomaly; under the condition of a reducing environment, a portion of Eu^{3+} is reduced to Eu^{2+} and separated from other REEs, which leads to a negative anomaly of Eu. Therefore, the Eu anomaly can be used as an indicator of a redox condition (Bau and Möller 1992). A Ce anomaly is generally affected by environmental pH and f_{O_2} and is more sensitive to pH (Elderfield and Sholkovitz 1987). The Ce in an oxidative environment mainly exists in the form of Ce^{4+}, and due to its low solubility, it is easily adsorbed and separated by hydroxides to produce negative anomalies.

In the Muli ore section, quartz in metallogenic stage shows positive Eu and negative Ce anomalies, indicating an oxidizing environment at this time. The pronounced negative Ce anomaly and the larger absolute value of the Eu anomaly in quartz from the late metallogenic stage indicate that the ore-forming fluids have a low temperature and a low f_{O_2} in the Muli ore section at the late metallogenic stage.

All metallogenic calcites from both the Muli and the Nadan ore sections display negative Eu and Ce anomalies, implying a constantly changing temperature and/or pH, and Eh of the ore-forming fluids (Feng et al. 2014; Qi et al. 2008). Because of the thermochemical reduction of Eu^{3+} to Eu^{2+} at elevated temperatures, the hydrothermal calcite will show a positive Eu anomaly if the crystallization temperature is below 200 °C. Above that temperature, minerals will display a negative Eu anomaly because the size of the Eu^{2+} ion prevents its incorporation into the calcite lattice during precipitation (Schwinn and Markl 2005). Therefore, the negative Eu anomaly of metallogenic

calcite in the Muli antimony deposit might indicate that the temperature of fluid systems is probably above 200 °C in the main metallogenic stage, which is consistent with our fluid inclusion study of calcites (unpublished).

5.4 Feasibilities of using the chondrite-normalized REE pattern to trace ore-forming fluids

The variability in REE composition observed within different gangue minerals indicates that significantly different conclusions can be drawn on tracing ore-forming fluids. In previous studies, the M-HREE can be enriched in the Fe–Mn bearing phase by sorption (Bau et al. 1996; Brugger and Meisser 2006). Wang et al. (2012b) reported that Fe + Mn (ppm) is negatively interrelated with the LREE/HREE ratios of calcites in the Banian deposit. Moreover, Wang et al. (2018) indicated that the Fe and Mn contents of ore-forming stage calcites are apparently higher than those of the calcites unrelated to mineralization in the Banqi Carlin-type gold deposit, and they are negatively correlated with the LREE/HREE ratio, which illustrates that the HREE concentrations of calcites are controlled by the incorporation of Fe and Mn. Based on the research above, we propose that the calcite with Fe–Mn impurities may not be suitable for tracing because of its preferential selectivity. Mao et al. (2006) suggested that the REE composition of pyrite mineral can be considered to be the reflection of the composition of pyrite fluid-inclusions and can be used to trace the sources and characteristics of the ore-forming fluids if the REE of the silicate phase in pyrite are not involved in REE analysis. Therefore, if pyrite is to be used to trace the ore-forming fluids, we should make sure that pyrite is not completely dissolved during sample pre-treatment. In addition, if single minerals with low trace element contents are to be used as a tracer, the purity of the sample should be ensured during pre-treatment. Wang et al. (2015) and Zheng et al. (2010, 2011) have reported the REE characteristics of arsenopyrite in the Bake gold deposit. The REE contents (excluding Y) of arsenopyrites determined by Wang et al. (2015) are 2.7–9.0 μg/g and those of wall rock are 401–490 μg/g, while those of arsenopyrites determined by Zheng et al. (2010, 2011) are 10.2–86.8 μg/g. The REE contents of arsenopyrites analysed by different researchers differ by an order of magnitude, which suggests that the higher values are likely caused by mixed contamination from wall rocks.

Although Gagnon et al. (2003) pointed out that significant, small-scale variation occurs in REE patterns on a fine scale; meanwhile, they suggested that LA-ICP-MS analysis can guarantee the high quality and precision of data. Considering that trace elements are very low in our samples, with some below the detection limit of LA-ICP-MS analysis, the digestion method was used in the present study.

In summary, there are many factors that restrict the distribution of REE in minerals and the chondrite-normalized REE pattern obtained by experiments. We should not only combine various minerals for a comprehensive study but also analyse the formation mechanisms of REE characteristics of various minerals when single minerals are used in tracing.

5.5 Characteristics of ore-forming fluids

Different REE patterns appear in various minerals in the Muli antimony deposit. No matter what the REE pattern is, it can reflect the fluid properties when its genetic mechanism is constrained. The fluid inclusions in quartz and pyrite in the metallogenic stage from the Muli ore section should record the information of ore-forming fluids directly (Mao et al. 2006, 2010). Both quartz and pyrite in the metallogenic period show the enrichment of LREE, indicative of fluids rich in LREE in the metallogenic stage of the Muli ore section. The REE pattern of the wall rock in the Muli section is similar to that of quartz and pyrite in the metallogenic period, which indicates that the wall rock material is involved in the mineralization of the Muli ore section. The tetrad effects of W-shaped quartz in the late metallogenic stage of the Muli ore section imply that the late stage hydrothermal fluids are derived from the highly evolved silicate magmas (Schönenberger et al. 2008; Takahashi et al. 2002).

Unique M-HREE-enriched calcite appears in antimony and gold deposits in the large-scale low-temperature epithermal metallogenic domain in southwestern China (Peng et al. 2004; Su et al. 2009; Wang et al. 2012b, 2018), but its genetic mechanism is still obscure. It has been shown that the REE partition pattern of modern hydrothermal fluids is an LREE-enriched type (Klinkhammer et al. 1994). Therefore, the REE patterns of ore-forming fluids of hydrothermal deposits occurring in continental crust should be more similar to the LREE enrichment type of crustal rocks (Peng et al. 2004). Thus, it is unlikely that the initial fluid in the metallogenic stage of the Nadan ore section was M-HREE rich. LREE-enriched minerals (i.e., monazite) preferentially or simultaneously precipitate with calcite, which preferentially traps LREEs in the fluid, resulting in serious LREE depletion in calcite (Chesley et al. 1991; Peng et al. 2004). However, no monazites have been reported so far. Schwinn and Markl (2005) reported that the REE patterns of granite leachates show a "roof-shaped" curvature (i.e., M-HREE enrichment), and the fractionation between LREE and HREE is significantly larger. M-HREE enriched calcite in the Muli antimony deposit may also indicate that fluids from granite

are involved in mineralization. Nevertheless, there are no magmatic rocks exposed in the Muli antimony deposit or even in the antimony and gold deposits in the large-scale low-temperature epithermal metallogenic domain in southwestern China. It remains unclear whether or not the M-HREE enriched pattern that implies antimony and gold mineralization is related to the concealed granite body. Alternatively, the authors suggested that Fe–Mn impurities in calcite may play an important role in the enrichment of M-HREEs at the metallogenic stage in the Nadan ore section (Wang et al. 2012b, 2018). In our study, all calcites that are precipitated at metallogenic stage have much higher Fe and Mn contents than those precipitated at post-metallogenic stage (unpublished). The preferential selectivity of Fe and Mn impurities resulted in the concentrated M-HREE of calcite in the metallogenic period of the Nadan ore section, while the post-metallogenic calcites from the Muli ore section are enriched in LREEs and their Fe and Mn contents (unpublished) are apparently lower than those of metallogenic calcites from the Nadan ore section. These observations indicate that under this condition, Fe and Mn impurities do not work and that the LREE/HREE fractionation of calcite is controlled by crystal chemistry (Rimstidt et al. 1998; Wood 1990; Wang et al. 2012b, 2018).

At present, the origin of the M-HREE enriched calcite is not fully understood, and the REE characteristics of various types of single minerals in Muli antimony deposit are different, so the method of tracing ore-forming fluid by REE distribution patterns of single minerals is invalid. The REE characteristics of various minerals in the same deposit should be considered. Moreover, we need to combine other methods to provide strong constraints on the source and evolution of the ore-forming fluids.

6 Conclusions

1. The M-HREE enriched calcite in the Muli antimony deposit is either affected by the Fe and Mn impurities or suggests that the mineralization is related to granite. The REE distribution patterns of quartz and pyrite in the metallogenic stage of Muli ore section are similar to those of wall rocks, indicating that the wall rock materials are involved in the mineralization. The quartz with an W-shaped REE pattern in the Muli ore section typically reflects a strong water–rock reaction with highly evolved granitic rocks. However, the different LREE/HREE and $(La/Yb)_N$ values in different minerals or in different stages of the same mineral, and various REE distribution patterns reveal that the ore-forming fluids have multiple stages and sources.
2. The positive Eu and negative Ce anomalies of quartz in the metallogenic stage of the Muli ore section indicate that the ore-forming environment is oxidative. The negative Ce and weaker Eu anomalies of quartz in the late metallogenic stage of the Muli ore section indicate that the temperature and f_{O_2} have decreased at this stage. The negative Eu anomaly of all metallogenic calcites in the Muli antimony deposit reveals that the ore-forming temperature of the main metallogenic stage is greater than 200 °C, and the fluid system is oxidative.
3. The observed REE geochemical characteristics from single minerals may not necessarily be indicative of the ore-forming fluids. It is necessary to fully understand the formation mechanism of the chondrite-normalized REE pattern in single minerals to trace ore-forming fluids, and various methods or the REE distribution patterns of various minerals should be combined.

Acknowledgements This research is jointly supported by the National Natural Science Foundation of China (Grant Nos. 41772070, 41303038), Open Fund of State Key Laboratory of Ore Deposit Geochemistry (201502). Special thanks are due to the geological engineers from the Yunnan Muli Antimony Industry Co., Ltd and Mr. Dazhou Chen for their enthusiastic help during our field investigation. We are grateful to Ms. Jing Hu and Ms. Yan Huang for their warmhearted experimental guidance and instrumentation support. We would like to thank Professors A.U. Ugarkar and Chuanwei Zhu, for their valuable suggestions and insightful comments on this manuscript.

References

Abedini A, Calagari AA, Naseri H (2016) Mineralization and REE geochemistry of hydrothermal quartz and calcite of the Helmesi vein-type copper deposit, NW Iran. Neues Jahrbuch für Geologie und Paläontologie-Abhandlungen 281(2):123–134

Bao GP, Cui YL, Gao JG (2013) REE geochemical features of hydrothermal calcite from Maozu Pb–Zn deposit, northeastern Yunnan province, China. Acta Mineral Sin 33(4):681–685

Bau M, Dulski P (1995) Comparative study of yttrium and rare-earth element behaviours in fluorine-rich hydrothermal fluids. Contrib Mineral Petrol 119(2–3):213–223

Bau M, Möller P (1992) Rare earth element fractionation in metamorphogenic hydrothermal calcite, magnesite and siderite. Mineral Petrol 45(45):231–246

Bau M, Koschinsky A, Dulski P, Hein JR (1996) Comparison of the partitioning behaviours of yttrium, rare earth elements, and titanium between hydrogenetic marine ferromanganese crusts and seawater. Geochim Cosmochim Acta 60(10):1709–1725

Bi XW, Hu RZ, Peng JT, Wu KX (2004) REE and HFSE geochemical characteristics of pyrites in Yao'an gold deposit: tracing ore forming fluid signatures. Bull Mineral Petrol Geochem 23(1):1–4

Brugger J, Meisser N (2006) Manganese-rich assemblages in the Barrhorn unit, Turtmanntal, central Alps, Switzerland. Can Mineral 44(1):229–248

Cao JC (1995) REE geochemical characteristics of epithermal vein fluorite deposits in south China. Geochimica 24(3):225–234

Cao HW, Zhang ST, Gao YZ, Ma Y, Zeng ZF, Gao F, Zou H (2014) REE geochemistry of fluorite from Linxi fluorite deposit and its geological implications, Inner Mongolia Autonomous Region. Geochimica 43(2):131–140

Chen MH, Wu LL, Phillip JU, Tony N, Zheng JM, Qin YZ (2007) REE features of arsenian pyrite and vein quartz and their fluid inclusions in the Jinfeng (Lannigou) gold deposit, Guizhou province, China. Acta Petrol Sin 23(10):2423–2433

Chesley JT, Halliday AN, Scrivener RC (1991) Samarium–neodymium direct dating of fluorite mineralization. Science 252(5008):949–951

Chesley JT, Halliday AN, Kyser TK, Spry PG (1994) Direct dating of MVT mineralization: use of Sm–Nd in fluorite. Econ Geol 89(5):1192–1199

Debruyne D, Hulsbosch N, Muchez P (2016) Unraveling rare earth element signatures in hydrothermal carbonate minerals using a source–sink system. Ore Geol Rev 72:232–252

Deng H, Huang ZL, Xiao XG, Ding W (2014) REE geochemistry of gangue calcite from Banpo deposit in Dushan antimony ore field, Guizhou province, China. Acta Mineral Sin 34(2):208–216

Dromgoole EL, Walter LM (1990) Iron and manganese incorporation into calcite: effects of growth kinetics, temperature and solution chemistry. Chem Geol 81(4):311–336

Elderfield H, Sholkovitz ER (1987) Rare earth elements in the pore waters of reducing nearshore sediments. Earth Planet Sci Lett 82(3–4):280–288

Fan JG, Ni P, Su WC, Qi L, Tian JH (2000) Characteristics and significance of rare earth elements in quartz of Sidaogou hydrothermal gold deposit, Liaoning. Acta Petrol Sin 16(4):587–590

Feng CX, Bi XW, Wu LY, Zou ZC, Tang YY (2011) Significance and characteristics of REE geochemistry in calcite in the eastern ore belt of the Baiyangping poly-metallic metallogenic province, northwestern Yunnan province, China. J Jilin Univ Earth Sci Ed 41(5):1397–1406

Feng CX, Bi XW, Liu S, Hu RZ (2014) Fluid inclusion, rare earth element geochemistry, and isotopic characteristics of the eastern ore zone of the Baiyangping polymetallic Ore district, northwestern Yunnan Province, China. J Asian Earth Sci 85(2):140–153

Gagnon JE, Samson IM, Fryer BJ et al (2003) Compositional heterogeneity in fluorite and the genesis of fluorite deposits: insights from LA-ICP-MS analysis. Can Mineral 41(2):365–382

Ghaderi M, Palin JM, Campbell IH, Sylvester PJ (1999) Rare earth element systematics in scheelite from hydrothermal gold deposits in the Kalgoorlie-Norseman region, Western Australia. Econ Geol 94(3):423–437

Han ZC, Wang JS, Gao ZH (2017) Geochemical characteristics and implications of REE, carbon and oxygen isotopes of calcite from La'e mercury deposit. J Kunming Univ Sci Technol Nat Sci Ed 42(3):28–37

Hazarika P, Mishra B, Pruseth KL (2016) Scheelite, apatite, calcite and tourmaline compositions from the late Archean Hutti orogenic gold deposit: Implications for analogous two stage ore fluids. Ore Geol Rev 72:989–1003

Hecht L, Freiberger R, Gilg HA, Grundmann G, Kostitsyn YA (1999) Rare earth element and isotope (C, O, Sr) characteristics of hydrothermal carbonates: genetic implications for dolomite-hosted talc mineralization at Göpfersgrün (Fichtelgebirge, Germany). Chem Geol 155(1–2):115–130

Huang DY, Lei WL (1997) The geological features and metallogenetic mechanism of Muli Sb deposit, Guangxi. Yunnan Geol 16(4):377–385

Huang ZL, Chen J, Han RS, Li WB, Gao DR, Zhao DS, Liu CQ (2001) REE geochemistry of calcite—a gangue mineral in the Huize ore deposit, Yunnan. Acta Mineral Sin 21(4):659–666

Huang JG, Li HJ, Li WJ, Dong L (2012) Element geochemistry of ore-bearing rock series in the Getang gold deposit, Guizhou Province. Geol China 39(5):1318–1326

Jiang YN (1988) The distribution characteristics of the rare earth elements in phyllites and iron-bearing quartzites form Anshan district. Contr Geol Miner Resour Res 3(1):23–31

Johannesson KH, Lyons WB, Yelken MA, Gaudette HE, Stetzenbach KJ (1996) Geochemistry of the rare-earth elements in hypersaline and dilute acidic natural terrestrial waters: Complexation behavior and middle rare-earth element enrichments. Chem Geol 133(1–4):125–144

Klinkhammer GP, Elderfield H, Edmond JM, Mitra A (1994) Geochemical implications of rare earth element patterns in hydrothermal fluids from mid-ocean ridges. Geochim Cosmochim Acta 58(23):5105–5113

Leng CB, Wang YH, Zhang XC, Gao JF, Zhang W, Xu XY (2018) Constraints of molybdenite Re–Os and scheelite Sm–Nd ages on mineralization time of the Kukaazi Pb–Zn–Cu–W deposit, Western Kunlun, NW China. Acta Geochim 37(1):47–59

Leybourne MI, Goodfellow WD, Dan RB, Hall GM (2000) Rapid development of negative Ce anomalies in surface waters and contrasting REE patterns in groundwaters associated with Zn–Pb massive sulphide deposits. Appl Geochem 15(6):695–723

Li B (1999) Origin of ore forming material of the Muli antimony deposit. Geol Explor Non-Ferr Met 8(2):103–106

Li HM, Shen YC, Mao JW, Liu TB, Zhu HP (2003) REE features of quartz and pyrite and their fluid inclusions: an example of Jiaojia-type gold deposits, northwestern Jiaodong peninsula. Acta Petrol Sin 19(2):267–274

Li XF, Wang G, Mao W, Wang CZ, Xiao R, Wang M (2015) Fluid inclusions, muscovite Ar–Ar age, and fluorite trace elements at the Baiyanghe volcanic Be–U–Mo deposit, Xinjiang, northwest China: implication for its genesis. Ore Geol Rev 64:387–399

Liang T, Wang DH, Qu WJ, Cai MH, Wei KL, Huang HM, Wu DC (2007) REE geochemistry of calcites in the Dachang tin-polymetallic deposit, Guangxi. Acta Petrol Sin 23(10):2493–2503

Lottermoser BG (1992) Rare earth elements and hydrothermal ore formation processes. Ore Geol Rev 7(1):25–41

Mao GZ, Hua RM, Gao JF, Long GM, Lu HJ, Li WQ, Zhao KD (2006) Existence of REE in different phases of gold-bearing pyrite in the Jinshan gold deposit, Jiangxi province. Acta Mineral Sin 26(4):409–418

Mao GZ, Hua RM, Gao JF, Zhao KD, Long GM, Lu HJ, Yao JM (2010) Rare earth element and trace element features of gold-bearing pyrite in the Jinshan Gold Deposit, Jiangxi Province. Acta Geologica Sinica 84(3):614–623

Moller P, Morteani G (1983) On the geochemical fractionation of rare earth elements during the formation of Ca-minerals and its application to problems of the genesis of ore deposits. Bulletin De Lacadémie Nationale De Médecine 152(28):747–791

Mucci A (1988) Manganese uptake during calcite precipitation from seawater: conditions leading to the formation of a pseudokutnahorite. Geochim Cosmochim Acta 52(7):1859–1868

Norman DI, Landis GP (1983) Source of mineralizing components in hydrothermal ore fluids as evidenced by $^{87}Sr/^{86}Sr$ and stable isotope data from the Pasto Bueno deposit, Peru. Econ Geol 78(3):451–465

Peng JT, Hu RZ, Jiang GH (2003) Samarium–neodymium isotopic system of fluorites from the Qinglong antimony deposit, Guizhou province: constraints on the mineralizing age and ore-forming materials' sources. Acta Petrol Sin 19(4):785–791

Peng JT, Hu RZ, Qi L, Zhao JH, Fu YZ (2004) REE distribution pattern for the hydrothermal calcites from the Xikuangshan antimony deposit and its constraining factors. Geol Rev 50(1):25–32

Peng JT, Fu YZ, Yuan SD, Shen NP, Zhang DL (2006) Sm–Nd isotope dating of some Ca-bearing minerals in hydrothermal deposits. Geol Rev 52(5):662–667

Pingitore NE Jr, Eastman MP, Sandidge M, Oden K, Freiha B (1988) The coprecipitation of manganese(II) with calcite: an experimental study. Mar Chem 25(2):107–120

Qi XX, Tian-Fu Li TF, Yu CL (2008) Rare earth element and trace element geochemistry of Shalagang antimony deposit in the southern tibet and its tracing significance for the origin of metallogenic elements. GeoSci 22(2):162–172

Rimstidt JD, Balog A, Webb J (1998) Distribution of trace elements between carbonate minerals and aqueous solutions. Geochim Cosmochim Acta 62(11):1851–1863

Roberts S, Palmer MR, Waller L (2006) Sm–Nd and REE characteristics of tourmaline and scheelite from the Björkdal gold deposit, northern Sweden: evidence of an intrusion-related gold deposit? Econ Geol 101(7):1415–1425

Schönenberger J, Köhler J, Markl G (2008) REE systematics of fluorides, calcite and siderite in peralkaline plutonic rocks from the Gardar province, South Greenland. Chem Geol 247(1–2):16–35

Schwinn G, Markl G (2005) REE systematics in hydrothermal fluorite. Chem Geol 216(3–4):225–248

Shen NP, Cai JL, Su WC, Dong WD (2015) Characteristics and source significance of trace element geochemistry of fluorite from Chashan Sb–W deposit in Guangxi. Acta Geol Sin 89(2):384–391

Su WC, Hu RZ, Xia B, Xia Y, Liu YP (2009) Calcite Sm–Nd isochron age of the Shuiyindong Carlin-type gold deposit, Guizhou, China. Chem Geol 258(3):269–274

Su WC, Dong WD, Zhang XC, Shen NP, Hu RZ, Hofstra AH, Cheng LZ, Xia Y, Yang KY (2018) Carlin-type gold deposits in the Dian-Qian-Gui "Gold Triangle" of Southwest China. Rev Econ Geol 20:157–185

Subías I, Fernández-Nieto C (1995) Hydrothermal events in the Valle de Tena (Spanish Western Pyrenees) as evidenced by fluid inclusions and trace-element distribution from fluorite deposits. Chem Geol 124(3–4):267–282

Takahashi Y, Yoshida H, Sato N, Hama K, Yusa Y, Shimizu H (2002) W- and M-type tetrad effects in REE patterns for water-rock systems in the Tono uranium deposit, central Japan. Chem Geol 184(3):311–335

Veksler IV, Dorfman AM, Kamenetsky M, Dulski P, Dingwell DB (2005) Partitioning of lanthanides and Y between immiscible silicate and fluoride melts, fluorite and cryolite and the origin of the lanthanide tetrad effect in igneous rocks. Geochim Cosmochim Acta 69(11):2847–2860

Wang LJ, Man KL (1994) Analysis of ore-control geological conditions of Muli antimony deposit, Guangnan. Yunnan Geol 13(2):133–138

Wang GZ, Hu RZ, Liu Y, Sun GS, Su WC, Liu H (2003) REE geochemical characteristics from fluorite in Qinglong antimony deposit, south-western Guizhou. J Mineral Petrol 23(2):62–65

Wang JS, Wen HJ, Shi SH (2010) Characteristics and implications of REE, carbon and oxygen isotopes of hydrothermal calcite from the mercury metallogenic belt in Hunan and Guizhou provinces, China. Acta Mineral Sin 30(2):185–193

Wang JJ, Hu YZ, Han RS (2011) Geochemical characteristics and its implications of trace elements in Qinglong antimony deposit, Guizhou province, China. Acta Mineral Sin 31(3):571–577

Wang DH, Li C, Chen ZH, Wang CH, Huang F, Qu WJ (2012a) New application of molybdenite in the study on ore deposits: rare earth elements geochemistry. J Jilin Univ Earth Sci Ed 42(6):1647–1655

Wang JS, Wen HJ, Fan HF, Zhu JJ (2012b) Sm–Nd geochronology, REE geochemistry and C and O isotope characteristics of calcites and stibnites from the Banian antimony deposit, Guizhou Province, China. Geochem J 46(5):393–407

Wang ZP, Xia Y, Song XY, You B, Zheng XH, Wang XY (2012c) Isotopes and REE characteristic and ore-forming materials source of the Taipingdong-Zimudang gold deposit. Acta Mineral Sin 32(1):93–100

Wang JS, Wen HJ, Li C, Jiang XJ, Zhu CW, Du SJ, Lei Z (2015) Determination of age and source constraints for the Bake quartz vein-type gold deposit in SE Guizhou using arsenopyrite Re–Os chronology and REE characteristics. Geochem J 49(1):73–81

Wang JS, Han ZC, Li C, Gao ZH, Yang Y, Zhou GC (2018) REE, Fe and Mn contents of calcites and their prospecting significance for the Banqi carlin-type gold deposit in southwestern China. Geotect Met 42(3):494–504

Whitney PR, Olmsted JF (1998) Rare earth element metasomatism in hydrothermal systems: the Willsboro–Lewis wollastonite ores, New York, USA. Geochim Cosmochim Acta 62(17):2965–2977

Wood SA (1990) The aqueous geochemistry of the rare-earth elements and yttrium: 2. Theoretical predictions of speciation in hydrothermal solutions to 350 °C at saturation water vapor pressure. Chem Geol 88(1–2):99–125

Yan SH, Wang AJ, Gao L, Zhao YQ, Chen GZ (2000) REE geochemistry and implications of stable isotopes in Dashui type gold deposits. Miner Depos 19(1):37–45

Yu KJ (1990) Geological characteristics and exploration experience on Yunnan antimony ores. Yunnan Geology 9(2):83–94

Zhang Y, Xia Y, Wang ZP, Yan BW, Fu ZK, Chen M (2010) REE and stable isotope geochemical characteristics of Bojitian gold deposit, Guizhou province. Geosci Front 17(2):385–395

Zhang XD, Yang RD, Wang W, Wei HR (2011) The geochemical characteristics and significance of trace element and REE in Pingqiu gold deposits, southeastern Guizhou. J Mineral Petrol 31(1):63–69

Zhang Y, Gu XX, Zhang YM, Cheng WB, Song YQ (2012) Geochemical characteristics of rare earth elements and its significance in the mineralization of quartz and pyrite in the Liubeigou gold deposit, Inner Mongolia. Bull Mineral Petrol Geochem 31(1):23–30

Zhao ZH, Masuda A, Shabani MB (1992) Tetrad effects of rare-earth elements in rare-metal granites. Geochimica 3:221–233

Zhao ZH, Xiong XL, Han XD, Wang YX, Wang Q, Bao ZW, Jahn B (2002) Controls on the REE tetrad effect in evidence from the Qianlishan and Baerzhe Granites, China. Geochem J 36(6):527–543

Zheng J, Yu DL, Yang ZQ (2010) A study on the trace element geochemical characteristics of pyrite and arsenopyrite in Bake gold deposit, east Guizhou province, P. R. China. Acta Mineral Sin 30(1):107–114

Zheng J, Yu DL, Wu WM, Yang ZQ, Liu Y (2011) Typomorphic characteristics of arsenopyrite in the Bake gold deposit, eastern Guizhou province. GeoSci 25(4):750–758

Zhou H, Greig A, Tang J, You CF, Yuan DX, Tong XN, Huang Y (2012) Rare earth element patterns in a Chinese stalagmite controlled by sources and scavenging from karst groundwater. Geochim Cosmochim Acta 75(1):1–18

Zhu JB, Fang WX, Liu JJ, Hu YZ (2010) The REE characteristics and genetic study of Qinglong antimony deposit, Guizhou. Contr Geol Miner Resour Res 25(2):118–123